Quantum Storage of a Photonic Polarization Qubit in a Solid

Mustafa Gündoğan,[1,*] Patrick M. Ledingham,[1] Attaallah Almasi,[1,†] Matteo Cristiani,[1] and Hugues de Riedmatten[1,2]
[1]*ICFO-Institut de Ciencies Fotoniques, Av. Carl Friedrich Gauss 3, 08860 Castelldefels (Barcelona), Spain*
[2]*ICREA-Institució Catalana de Recerca i Estudis Avançats, 08015 Barcelona, Spain*
(Received 18 January 2012; published 10 May 2012)

We report on the quantum storage and retrieval of photonic polarization quantum bits onto and out of a solid state storage device. The qubits are implemented with weak coherent states at the single photon level, and are stored for a predetermined time of 500 ns in a praseodymium doped crystal with a storage and retrieval efficiency of 10%, using the atomic frequency comb scheme. We characterize the storage by using quantum state tomography, and find that the average conditional fidelity of the retrieved qubits exceeds 95% for a mean photon number $\mu = 0.4$. This is significantly higher than a classical benchmark, taking into account the Poissonian statistics and finite memory efficiency, which proves that our crystal functions as a quantum storage device for polarization qubits. These results extend the storage capabilities of solid state quantum light matter interfaces to polarization encoding, which is widely used in quantum information science.

DOI: 10.1103/PhysRevLett.108.190504 PACS numbers: 03.67.Hk, 42.50.Ex, 42.50.Gy, 42.50.Md

The ability to transfer quantum information in a coherent, efficient and reversible way from light to matter plays an important role in quantum information science [1]. It enables the realization of photonic quantum memories (QM) [2] which are required to render scalable elaborate quantum protocols involving many probabilistic processes that have to be combined. A prime example is the quantum repeater [3–5], where quantum information can be distributed over very long distances. Other applications include quantum networks [6], linear optics quantum computation [7], deterministic single photon sources [8] and multiphoton quantum state engineering.

Proof of principle experiments demonstrating photonic QMs have been reported in different atomic systems such as cold [9–15] and hot atomic gases [16–19], single atoms in cavities [20] and solid state systems [21,22]. In recent years, solid state atomic ensembles implemented with rare-earth doped solids have emerged as a promising system to implement QMs. They provide a large number of atoms with excellent coherence properties naturally trapped into a solid state system. In addition, they feature a static inhomogeneous broadening that can be shaped at will, enabling new storage protocols with enhanced storage properties (e.g., temporal multiplexing) [23,24]. Finally, some of the rare-earth doped crystals (e.g., praseodymium and europium doped crystals) possess ground states with extremely long coherence times [25] (> seconds), which hold promise for implementing long lived solid state quantum memories.

Recent progress towards solid state QMs include the storage of weak coherent pulses at the single photon level [21,26–28], the quantum storage of coherent pulses with efficiency up to 70% [22], the spin-state storage of bright coherent pulses [25,29] and the storage of multiple temporal modes in one crystal [30,31]. Very recently, these capabilities have been extended to the storage of nonclassical light generated by spontaneous down conversion, leading to the entanglement between one photon and one collective atomic excitation stored in the crystal [32,33], entanglement between two crystals [34] and time-bin qubit storage [35].

All previous experiments towards solid state QMs have been so far limited to the storage of multiple modes using the time degree of freedom, e.g., time bin or energy time qubits. However, quantum information is very often encoded in the polarization states of photons, which provide an easy way to manipulate and analyze the qubits. Extending the storage capabilities of solid state QMs to polarization encoded qubits would thus bring much more flexibility to this kind of interface. Unfortunately, storing coherently polarization states is not straightforward in rare-earth doped crystals. The main difficulty is that these crystals are in general birefringent and have a strongly polarization dependent absorption. Storing directly a polarization qubit in such a system would result in a severely degraded fidelity of the retrieved qubits.

In this paper, we report on the storage and retrieval of a photonic polarization qubit into and out of a solid state quantum storage device with high conditional fidelity. The photonic qubits are implemented with weak coherent pulses of light, with a mean photon number μ ranging from 0.01 to 36. We measure the conditional fidelity [2] of the storage and retrieval process (i.e., assuming that a photon was reemitted) and compare it to classical benchmarks. With this procedure, we can show that our crystal behaves as a quantum storage device, even if tested with classical, weak coherent pulses. We overcome the difficulty of anisotropic absorption by splitting the polarization components of the qubit and storing them in two spatially separated ensembles within the same crystal [12,36,37].

Our device is implemented using a 3 mm long $Pr^{3+}:Y_2SiO_5$ crystal (0.05%). The relevant atomic transition connects the $^3H_4$ ground state to the $^1D_2$ excited state and has a wavelength of 605.977 nm. Each state has three hyperfine sublevels as shown in Fig. 1. The measured maximal optical depth at the center of the 5 GHz inhomogeneous line is 7. We use the atomic frequency comb (AFC) scheme to store and retrieve the qubits [24]. This requires to shape the inhomogeneous absorption profile into a series of periodic and narrow absorbing peaks, placed in a wide transparency window. This creates a frequency grating and when a photon is absorbed by the comb, it will be diffracted in time and reemitted after a predetermined time $t_S = 1/\Delta$, where Δ is the spacing between absorption peaks. Although in our experiment the storage time is predetermined by the comb spacing, $Pr^{3+}:Y_2SiO_5$ has an appropriate level structure which would allow the transfer of the excitation to a spin-state enabling longer storage times and on demand read-out [29].

Our experimental apparatus is described in Fig. 1. The laser source to generate light at 606 nm is based on sum frequency generation (SFG) in a PP-KTP waveguide (AdVR corp) from two amplified laser diodes at 1570 nm

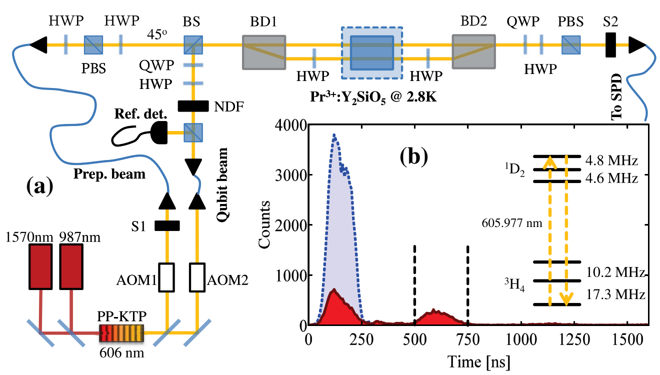

FIG. 1 (color online). (a) Experimental setup. The preparation beam and the qubit beam are derived from the same laser at 606 nm. Both beams are amplitude and frequency modulated using an acousto-optic modulator (AOM). The polarization of the qubit beam can be set arbitrarily with a half wave plate (HWP) and a quarter wave plate (QWP). The qubit beam is attenuated down to the single photon level using neutral density filters (NDF). The two beams are recombined at a beam splitter (BS) and sent to the storage device which is composed of the crystal, two beam displacers (BD) and two HWP. The light released by the crystal is then sent to a polarization analyzer, before being detected with a single photon detector (SPD). The two mechanical shutters (S1 and S2) are used to suppress optical noise from the preparation beam and to protect the SPD. (b) Storage and retrieval of a weak $|V\rangle$ qubit with duration 140 ns and $\mu = 0.4$. The temporal histogram of the detection without (dotted line, through a transparency window) and with (solid line) AFC is shown. The dashed lines around the AFC echo show the detection window. Inset: Level scheme of $Pr^{3+}:Y_2SiO_5$ with the dashed arrows showing the relevant transition for photon absorption and reemission.

(Toptica, DL 100 and Keopsys fiber amplifier) and 987 nm (Toptica, TA pro). With input power of 370 mW and 750 mW for the 987 nm laser and 1570 nm laser, respectively, we achieve an output power of 90 mW at 606 nm. Taking into account the 30% coupling efficiency of both beams into the waveguide, we obtain a SFG efficiency of $\sim 350\% W^{-1}$. The laser linewidth estimated by spectral hole burning experiments is <400 kHz. The beam is then split in two parts, one which will be used for the memory preparation (preparation beam) and one to prepare the weak pulses to be stored (qubit beam). In each path, the amplitude of the light is modulated with an acousto-optic modulator (AOM) in a double pass configuration, in order to create the required sequence of pulses for the preparation of the memory and of the polarization qubits. The radio-frequency signals used to drive the AOMs are generated by an arbitrary waveform generator (500×10^6 sample/s, 200 MHz, 1 GB internal memory, PXIe module and ProcessFlow software from Signadyne). After the AOMs, both beams are coupled to a polarization maintaining optical fiber and sent to another optical table where the cryostat is located.

The crystal is cooled down to 2.8 K in a cryofree cooler (Oxford Instruments V14). After the fibers, the preparation beam is collimated to a diameter of around 600 μm with a telescope and sent to the storage device. Right before the cryostat, a beam displacer (BD1) splits the two polarization components of the incoming light onto two parallel spatial modes separated by 2.7 mm, copropagating through the crystal. To ensure equal power in both spatial modes, the polarization of the preparation beam is set to 45°. After BD1, the polarization of the horizontal beam (lower beam in Fig. 1) is rotated by 90° using a HWP such that both beams enter the crystal with the same polarization which is parallel to the D2 axis of the crystal, which maximizes the absorption. The qubit beam is strongly attenuated by a set of fixed and variable neutral density filters (NDF), and μ before BD1 was varied from 0.01 to 36. After the NDF, arbitrary polarization qubits are prepared, using a quarter (QWP) and a half wave plate (HWP). The qubits are then overlapped to the preparation beam at a beam splitter (BS). After the cryostat, we rotate back the polarization of the lower beam and the two spatial modes are combined again at a second beam displacer (BD2). The two path between BD1 and BD2 form an interferometer with very high passive stability [12,37].

After the interferometer, the transmitted and retrieved light enters the polarization analysis stage, composed of a QWP, a HWP and a polarization beam splitter (PBS), which allow us to measure the polarization in any basis. The transmitted beam at the PBS is coupled in a multimode fiber and sent to a silicon avalanche photodiode single photon detector (SPD, model Count, Laser Components). The electronic signal from the SPD is finally sent to a time stamping card (PXIe card from Signadyne) in order to record the arrival time histogram. The mean photon number μ is determined by measuring the detection probability per pulse p_{det} when no atoms are present (i.e., with the laser 60 GHz off resonance), and backpropagating before BD1 taking into account the detection efficiency ($\eta_D = 50\%$) and the transmission from before BD1 to the detector ($\eta_t = 40\%$). The preparation beam and the qubits are sent sequentially towards the crystal. The total experimental sequence lasts 3 s, during which the preparation lasts 1 s. During the next 2 s, 10^5 weak pulses are prepared, stored, and retrieved at a rate of 50 kHz.

In order to create the AFC, we first create a wide transparency window within the 5 GHz inhomogeneous profile. This is achieved by sending a series of pulses of duration 1.1 ms, during which the frequency of the light is swept linearly over a range of 12 MHz. The AFC is then created using the burn back procedure introduced in Ref. [38]. Four 2 ms long burn back pulses are sent with different frequencies separated by the comb spacing, leading to a 4-tooth comb.

As a first experiment, we verified that a complete set of qubit distributed over the Poincaré sphere could be stored and retrieved in the AFC. We set the comb spacing to 2 MHz, to give a storage time of 500 ns and we used the following input states: $|H\rangle$, $|V\rangle$, $|D\rangle = \frac{1}{\sqrt{2}}(|H\rangle + |V\rangle)$, $|A\rangle = \frac{1}{\sqrt{2}}(|H\rangle - |V\rangle)$, $|R\rangle = \frac{1}{\sqrt{2}}(|H\rangle + i|V\rangle)$, and $|L\rangle = \frac{1}{\sqrt{2}}(|H\rangle - i|V\rangle)$. Figure 1(b) shows the experimental storage of a $|V\rangle$ qubit encoded onto a pulse of duration 140 ns (FWHM) and with $\mu = 0.4$. Similar curves are obtained for the other states, and the average storage and retrieval efficiency is $\eta_M = (10.6 \pm 2.3)\%$. In order to test that the coherence between the $|H\rangle$ and $|V\rangle$ components of the qubits is preserved during the storage and retrieval, we then recorded the number of counts in the retrieved pulses when rotating the detection polarization basis using a HWP, for various input states. In Fig. 2(a), the curves obtained for $|V\rangle$ and $|D\rangle$ are shown. We observe interference fringes, with a raw fitted visibility of $(97 \pm 0.5)\%$ for the $|V\rangle$ qubit, and $(83 \pm 2)\%$ for the $|D\rangle$ qubit. In the case of a perfect circular $|R\rangle$ qubit, we should observe no dependance on the HWP angle when no QWP is inserted. The interference should be restored however, when a QWP is inserted before the HWP, which turns circular polarization into a linear one. The results are shown in Fig. 2(b). We indeed observe a strongly reduced visibility without the HWP ($(15 \pm 3)\%$), while a fringe with a high visibility of $(89 \pm 2)\%$ is obtained with the QWP. The residual visibility without the QWP may be due to a non perfect preparation of the $|R\rangle$ state. The non perfect visibility for the $|D\rangle$ and $|R\rangle$ is mostly due to small phase fluctuations engendered by mechanical vibrations from the cryostat. Indeed, we observe similar visibilities (99%, 98.5%, and 89% for $|H\rangle$, $|V\rangle$ and $|D\rangle$, respectively) for bright pulses out of resonance with the atomic transition. These results show that the phase between the two polarization components stored in different spatial modes is well preserved in the storage and retrieval process.

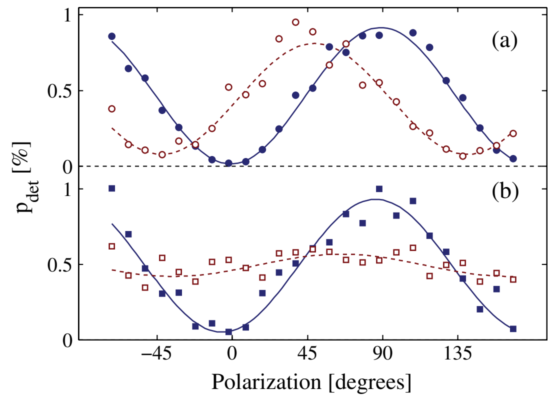

FIG. 2 (color online). (a) Measured detection probability (p_{det}) as a function of the polarizer angle, for $|V\rangle$ (filled circles) and $|D\rangle$ (open circles) input polarization qubits, with $\mu = 0.4$. The fitted raw visibilities are $(97 \pm 0.5)\%$ and $(83 \pm 2)\%$, respectively. (b) p_{det} as a function of polarization angle for $|R\rangle$ polarization qubit input, with (filled squares, $(89 \pm 2)\%$) and without (open squares, $(15 \pm 3)\%$) QWP inserted before the polarizer.

In order to better characterize the quality of the storage process, we reconstruct the density matrix of the retrieved qubits using quantum state tomography [39], for the complete set of qubits described above, with $\mu = 0.4$. The reconstructed output density matrices ρ_{out} for $|H\rangle$, $|D\rangle$ and $|R\rangle$ are shown in Fig. 3. From the matrices ρ_{out}, we can then estimate the conditional fidelity of the output states with respect to the target state $F^c_{|\psi\rangle} = \langle\psi|\rho_{\mathrm{out}}|\psi\rangle$. The values for the complete set of inputs are listed in Table I. We find a mean fidelity of $F^c_{\mathrm{mean}} = (96 \pm 2)\%$. We emphasize that this value is a lower bound for the conditional fidelity, since it is calculated with respect to a target state and also takes into account imperfections in the preparation of the qubits.

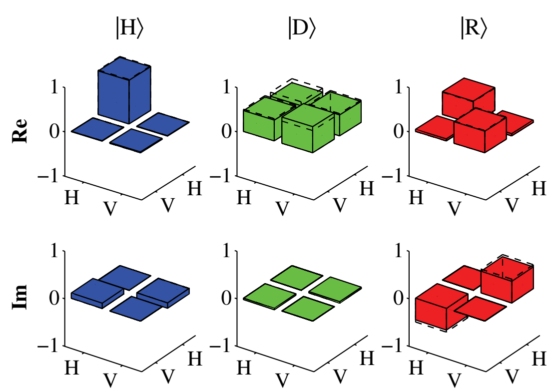

FIG. 3 (color online). Quantum state tomography. Reconstructed density matrices of the retrieved qubits for $|H\rangle$, $|D\rangle$ and $|R\rangle$ input qubits, with $\mu = 0.4$. No background has been subtracted.

TABLE I. Raw conditional fidelities for 6 different polarization input states. For this measurement, η_M varied between 8% and 10%. The errors have been obtained using Monte Carlo simulation taking into account the statistical uncertainty of photon counts and a technical error reflecting slow drifts in our systems, and estimated from the residuals from the fit of Fig. 2 and similar curves.

Input State	Fidelity	Input State	Fidelity
$\lvert H\rangle$	0.982 ± 0.003	$\lvert V\rangle$	0.983 ± 0.002
$\lvert D\rangle$	0.968 ± 0.005	$\lvert A\rangle$	0.938 ± 0.009
$\lvert R\rangle$	0.954 ± 0.007	$\lvert L\rangle$	0.926 ± 0.01

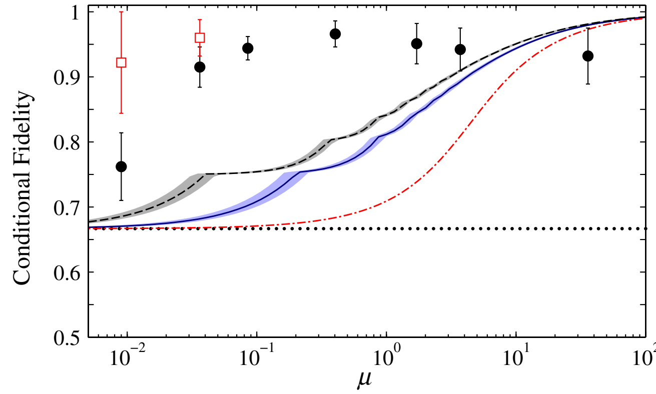

FIG. 4 (color online). Average fidelity measured as a function of the mean number of photon per pulse μ. The fidelity is measured by quantum state tomography and is the average of 3 input states $\lvert V\rangle$, $\lvert D\rangle$, and $\lvert R\rangle$. Filled circles are experimental data without any background subtraction. Empty squares correspond to dark count subtracted fidelities. The error takes into account statistical uncertainty of photon counts, technical errors and standard deviation of fidelities for the 3 polarizations. The various lines correspond to classical thresholds for different situations. The horizontal line is the limit of 2/3 for single qubits ($N = 1$). The dashed-dotted line corresponds to Eq. (1) where the Poissonian distribution of photon number is taken into account. Finally, the two other lines correspond to the cases where the finite storage efficiency is taken into account. The solid line corresponds to $\eta = (10 \pm 2)\%$. Measured η_M are between 8 and 10% for all points. The dashed line corresponds to $\eta = \eta_M \eta_t \eta_D = 2\%$. For $\mu > 1$, an additional ND filter is placed before the detector to avoid saturation effects.

Finally, in order to assess the quantum nature of the storage, we determine the average fidelity as a function of μ, and compare it with the best obtainable fidelity using a purely classical method consisting of measuring the state and storing the result in a classical memory. It has been shown that for a state containing N qubits, the best classical strategy leads to a fidelity of $F_c = (N+1)/(N+2)$ [40]. If the qubit is encoded in a weak coherent state, as it is the case in our experiment, one has to take into account the Poissonian statistics of the number of photons [20], and the classical fidelity is given by

$$F_{\text{class}}(\mu) = \sum_{N\geq 1} \frac{N+1}{N+2} \frac{P(\mu, N)}{1 - P(\mu, 0)}, \tag{1}$$

where $P(\mu, N) = e^{-\mu}\mu^N/N!$. This is valid for the case of a memory with unity efficiency. If $\eta_M < 1$, the classical memory could use a more elaborate strategy to take advantage of finite efficiency in order to gain more information about the input quantum state [20]. For example the classical memory could give an output only when the number of photons per pulse is high, and hence estimate with better fidelity the quantum state [41]. The different curves corresponding to the discussed cases are plotted in Fig. 4 as a function of μ. The points correspond to experimental data. Measured F^c_{mean} are significantly higher than the classical fidelity, for most of the photon numbers tested. This proves that our crystal performs as a quantum storage device for polarization qubits. We observe that the measured raw fidelity decreases for $\mu < 0.1$. This is mainly due to the dark count of the SPD, as high fidelities can be recovered by subtraction of this background (open squares). We also observe that when μ becomes too large ($\mu \geq 3.5$ in our case), the measured fidelity is not sufficient to be in the quantum regime. This analysis shows that very high fidelities are required to assess the quantum character of the storage when using coherent states with $\mu \gg 1$. To our knowledge, it is the first time that ensemble based storage has been characterized using this criteria.

The storage time in our experiment is limited by the minimal achievable width of the AFC peaks ($<$ 600 kHz), which is in turn limited by the linewidth of our unstabilized laser. The narrowest peaks that have been demonstrated so far in Pr^{3+}:Y_2SiO_5 have widths around 30 kHz [42]. The fundamental limit however is given by the homogeneous linewidth of the optical transition (2–3 kHz). This should allow a storage time in the excited state of a few tens of microseconds. This would enable the storage of multiple polarization qubits in the time domain. Moreover, the possibility of transferring the optical excitation to long lived spin excitation could increase the storage time to the order of seconds [25].

We have demonstrated the quantum storage and retrieval of polarization qubits implemented with weak coherent pulses at the single photon level, in a solid state storage device. The conditional fidelity of the storage and retrieval is >95%, significantly exceeding the classical benchmark calculated for weak coherent pulses and finite storage efficiency. We thus show that solid state quantum light matter interfaces are compatible with photonic polarization qubits, which are widely used in quantum information science. This significantly extends the storage capabilities of these types of memories. By combining the time and polarization degrees of freedom one could readily double the number of modes that can be stored in the memory and create quantum registers for polarization qubits. Using these resources, it may also be possible to design a quantum memory for complex light states such as hyperentangled states. In addition, as in our experiment the two polarization modes are stored in different spatial modes within the same crystal, our results also show that rare-earth doped crystals can serve as multimode spatial memories in the quantum regime.

We thank Stephan Ritter and Antonio Acin for interesting discussions regarding the classical benchmark, and the company Signadyne for technical support. Financial support by the European projects CHIST-ERA QScale and Marie Curie ITN CIPRIS, as well as by the ERC Starting Grant QuLIMA is acknowledged.

Note added.—We note that similar works demonstrating polarization qubit storage in neodymium doped crystals have been performed independently [43,44].

*mustafa.gundogan@icfo.es
†Present address: Department of Physics and Astronomy and LaserLaB, VU Amsterdam, Amsterdam, 1081HV, The Netherlands.

[1] K. Hammerer, A. S. Sørensen, and E. S. Polzik, Rev. Mod. Phys. **82**, 1041 (2010).
[2] C. Simon *et al.*, Eur. Phys. J. D **58**, 1 (2010).
[3] H.-J. Briegel, W. Dür, J. I. Cirac, and P. Zoller, Phys. Rev. Lett. **81**, 5932 (1998).
[4] L.-M. Duan, M. D. Lukin, J. I. Cirac, and P. Zoller, Nature (London) **414**, 413 (2001).
[5] N. Sangouard, C. Simon, H. de Riedmatten, and N. Gisin, Rev. Mod. Phys. **83**, 33 (2011).
[6] H. J. Kimble, Nature (London) **453**, 1023 (2008).
[7] P. Kok, W. J. Munro, K. Nemoto, T. C. Ralph, J. P. Dowling, G. J. Milburn, Rev. Mod. Phys. **79**, 135 (2007).
[8] D. N. Matsukevich, T. Chanelière, S. D. Jenkins, S.-Y. Lan, T. A. B. Kennedy, and A. Kuzmich, Phys. Rev. Lett. **97**, 013601 (2006).
[9] T. Chanelière, D. N. Matsukevich, S. D. Jenkins, S.-Y. Lan, T. A. B. Kennedy, and A. Kuzmich, Nature (London) **438**, 833 (2005).
[10] C. W. Chou, H. de Riedmatten, D. Felinto, S. V. Polyakov, S. J. van Enk, and H. J. Kimble, Nature (London) **438**, 828 (2005).
[11] J. Simon, H. Tanji, J. K. Thompson, and V. Vuletic, Phys. Rev. Lett. **98**, 183601 (2007).
[12] K. S. Choi, H. Deng, J. Laurat, and H. J. Kimble, Nature (London) **452**, 67 (2008).
[13] B. Zhao *et al.*, Nature Phys. **5**, 95 (2009).
[14] A. G. Radnaev, Y. O. Dudin, R. Zhao, H. H. Jen, S. D. Jenkins, A. Kuzmich, and T. A. B. Kennedy, Nature Phys. **6**, 894 (2010).
[15] H. Zhang *et al.*, Nature Photon. **5**, 628 (2011).
[16] B. Julsgaard, J. Sherson, J. I. Cirac, J. Fiurášek, and E. S. Polzik, Nature (London) **432**, 482 (2004).
[17] M. D. Eisaman, A. André, F. Massou, M. Fleischhauer, A. S. Zibrov, and M. D. Lukin, Nature (London) **438**, 837 (2005).
[18] K. F. Reim, P. Michelberger, K. C. Lee, J. Nunn, N. K. Langford, and I. A. Walmsley, Phys. Rev. Lett. **107**, 053603 (2011).
[19] M. Hosseini, G. Campbell, B. M. Sparkes, P. K. Lam, and B. C. Buchler, Nature Phys. **7**, 794 (2011).
[20] H. P. Specht, C. Nölleke, A. Reiserer, M. Uphoff, E. Figueroa, S. Ritter, and G. Rempe, Nature (London) **473**, 190 (2011).
[21] H. de Riedmatten, M. Afzelius, M. U. Staudt, C. Simon, and N. Gisin, Nature (London) **456**, 773 (2008).
[22] M. P. Hedges, J. J. Longdell, Y. Li, and M. J. Sellars, Nature (London) **465**, 1052 (2010).
[23] B. Kraus, W. Tittel, N. Gisin, M. Nilsson, S. Kröll, and J. I. Cirac, Phys. Rev. A **73**, 020302 (2006).
[24] M. Afzelius, C. Simon, H. de Riedmatten, and N. Gisin, Phys. Rev. A **79**, 052329 (2009).
[25] J. J. Longdell, E. Fraval, M. J. Sellars, and N. B. Manson, Phys. Rev. Lett. **95**, 063601 (2005).
[26] M. Sabooni, F. Beaudoin, A. Walther, N. Lin, A. Amari, M. Huang, and S. Kröll, Phys. Rev. Lett. **105**, 060501 (2010).
[27] T. Chanelière, J. Ruggiero, M. Bonarota, M. Afzelius, and J.-L. Le Gouët, New J. Phys. **12**, 023025 (2010).
[28] B. Lauritzen, J. Minář, H. de Riedmatten, M. Afzelius, N. Sangouard, C. Simon, and N. Gisin, Phys. Rev. Lett. **104**, 080502 (2010).
[29] M. Afzelius *et al.*, Phys. Rev. Lett. **104**, 040503 (2010).
[30] I. Usmani, M. Afzelius, H. de Riedmatten, and N. Gisin, Nature Commun. **1**, 12 (2010).
[31] M. Bonarota, J.-L. L. Gouët, and T. Chanelière, New J. Phys. **13**, 013013 (2011).
[32] C. Clausen, I. Usmani, F. Bussières, N. Sangouard, M. Afzelius, H. de Riedmatten, and N. Gisin, Nature (London) **469**, 508 (2011).
[33] E. Saglamyurek, N. Sinclair, J. Jin, J. A. Slater, D. Oblak, F. Bussières, M. George, R. Ricken, W. Sohler, and W. Tittel, Nature (London) **469**, 512 (2011).
[34] I. Usmani, C. Clausen, F. Bussières, N. Sangouard, M. Afzelius, and N. Gisin, Nature Photon. **6**, 234 (2012).
[35] E. Saglamyurek *et al.*, Phys. Rev. Lett. **108**, 083602 (2012).
[36] D. N. Matsukevich and A. Kuzmich, Science **306**, 663 (2004).
[37] C. W. Chou, J. Laurat, H. Deng, K. S. Choi, H. de Riedmatten, D. Felinto, and H. J. Kimble, Science **316**, 1316 (2007).
[38] M. Nilsson, L. Rippe, S. Kröll, R. Klieber and D. Suter, Phys. Rev. B **70**, 214116 (2004).
[39] D. F. V. James, P. G. Kwiat, W. J. Munro, and A. G. White, Phys. Rev. A **64**, 052312 (2001).
[40] S. Massar and S. Popescu, Phys. Rev. Lett. **74**, 1259 (1995).
[41] See Supplemental Material at http://link.aps.org/supplemental/10.1103/PhysRevLett.108.190504 for details.
[42] G. Hétet, J. J. Longdell, A. L. Alexander, P. K. Lam, and M. J. Sellars, Phys. Rev. Lett. **100**, 023601 (2008).
[43] C. Clausen, F. Bussières, M. Afzelius, and N. Gisin, preceding Letter, Phys. Rev. Lett. **108**, 190503 (2012).
[44] Z. Q. Zhou, W.-B. Lin, M. Yang, C.-F. Li, and G.-C. Guo, following Letter, Phys. Rev. Lett. **108**, 190505 (2012).